Pergamon

Ocean Engng, Vol. 21, No. 7, pp. 645–662, 1994

0029–8018/94 $7.00 + .00

NUMERICAL CALCULATION OF FORCES INDUCED BY SHORT-CRESTED WAVES ON A VERTICAL CYLINDER OF ARBITRARY CROSS-SECTION

SONGPING ZHU and G. MOULE

Department of Mathematics, The University of Wollongong, Wollongong, NSW 2500, Australia

Abstract—Most off-shore oil platforms are supported by vertical cylinders extending to the ocean floor. An important problem in off-shore engineering is the calculation of the wave loading exerted on these vertical cylinders. Analytical solutions have been found for the case of plane incident waves incident on a circular cylinder by MacCamy and Fuchs [(1954), Wave forces on piles: a diffraction theory. U.S. Army Corps of Engineering, Beach Erosion Board, Technical Memorandum No. 69] and also for short-crested waves incident on a circular cylinder by Zhu [(1993), Diffraction of short-crested waves around a circular cylinder. *Ocean Engng* **20**, 389–407]. However, for a cylinder of arbitrary cross-section, no analytic solutions currently exist. Au and Brebbia [(1983), Diffraction of water waves for vertical cylinders using boundary elements. *Appl. Math. Modelling* **7**, 106–114] proposed an efficient numerical approach to calculate the wave loads induced by plane waves on vertical cylinders by using the boundary element method. However, wind-generated waves are better modelled by short-crested waves. Whether or not these short-crested waves can induce larger wave forces on a structure is of great concern to ocean engineers. In this paper wave loads, induced by short-crested incident waves, on a vertical cylinder of arbitrary cross-section are discussed. For a cylinder of certain cross-section, the wave loads induced by short-crested waves can be larger than those induced by plane waves with the same total wave number.

1. INTRODUCTION

WAVE FORCES, among other forces such as current-induced drag forces, on off-shore structures are the major contribution to the total forces experienced by such structures, particularly in rough weather. The calculation of the wave loads on vertical cylinders is always of major concern to ocean engineers, especially recently when such studies are motivated by the need to build solid off-shore structures in connection with oil and natural gas productions. However, wind-generated waves in oceans are much better modelled by short-crested waves than by plane waves, and yet most of the previous works were mainly concentrated on wave loads induced by plane waves on solid structures, except the study carried out by Zhu (1993) on the diffraction of short-crested waves on a circular cylinder. Zhu (1993) found that wave loads induced by short-crested waves on a circular cylinder are always less than those induced by plane waves with the same total wave number. Due to the failure of Zhu's analytical solution when applied to a cylinder of cross-section other than a circle, an interesting and significant question remains to be answered. That is, can short-crested waves produce larger wave forces on a cylinder of non-circular cross-section than those produced by plane waves with the same total wave number? In this paper, we aim to provide a definite answer to this question by studying the wave loads induced by short-crested waves on a cylinder of arbitrary cross-section.

It is well known that wave forces on vertical cylinders can be calculated by using the Morrison equation if incident waves have wavelengths much greater than the cross-sectional dimensions of the cylinders; wave diffraction effects are ignored. However, when the wavelength of the incident waves is of the same order as the dimensions of the cylinder cross-section, the reflection and diffraction effects must be considered in determining the wave-induced forces on the cylinders. MacCamy and Fuchs (1954) found an analytic solution for the diffraction of plane waves around a vertical circular cylinder. Their results have been verified by many experimentalists such as Chakrabarti and Tam (1975) and Neelamani *et al.* (1989), and have shown good agreement with experimental data for $0.2 < \kappa a < 0.65$. Goda and Yoshimura (1972) found an analytic solution for the diffraction of plane waves around an elliptical cylinder by solving the Helmholtz equation using separation of variables. However, for the diffraction of waves around a vertical cylinder of arbitrary cross-section no analytic solution has been found. Numerical solutions are required for the analysis of the diffraction of waves around cylinders of arbitrary cross-sections.

Numerical solutions to the wave diffraction problems can be classified into two major classes: (a) the integral-equation method; (b) the hybrid-element method (see Mei, 1978). Earlier works on harbour oscillation problems, which are mathematically similar problems to wave diffraction around solid structures, were carried out by Banaugh and Goldsmith (1963), Hwang and Tuck (1970) and Lee (1971) by using the integral-equation method. In the later 1970s and earlier 1980s, the hybrid-element method became popular. Among other researchers, Chen and Mei (1974), Yue *et al.* (1976), Bettess and Zienkiewicz (1977), Houston (1981), Tsay and Liu (1983) and Tsay *et al.* (1989) all presented computational examples after hybrid elements were adopted in their calculations. However, the use of hybrid elements seems to be computationally very expensive; large computers such as CRAY-1 (e.g. Houston, 1981) were needed to carry out calculations. This is especially so when the wavelengths of the incident waves are short; a large number of elements are needed in order to resolve waves within a wavelength (Mei, 1978). With the advent of large computers, the boundary element method (BEM) was developed based on the theory of integral equations. A benchmark book was written by Brebbia *et al.* (1984). For water wave diffraction problems, Au and Brebbia (1983) used the BEM to calculate wave-induced forces on cylinders of various cross-sections (circular, elliptical and square) in water of constant depth for plane incident waves. Since only the boundaries of the problem need to be discretized, the dimension of the problem in computation reduces by one, leaving a system of equations of a size which can be solved in a reasonable time, even on personal computers. This results in a very efficient method for calculating the wave loads on vertical cylinders of arbitrary cross-sections.

Waves generated by winds blowing across the surface of oceans are modelled more accurately by short-crested waves than by plane waves. Short-crested waves are the waves of finite lateral extent, and exhibit different properties to plane waves, especially the nonlinear short-crested waves (see Jeffreys, 1924; Fuchs, 1952; Hsu *et al.*, 1979). Short-crested waves incident on a vertical cylinder will diffract and be reflected in a much more complicated manner than plane waves, and hence the effect on the wave loading on vertical cylinders is much harder to anticipate. Although an analytic solution was found by Zhu (1993) for short-crested waves incident on a circular cylinder and

wave forces induced by these short-crested waves were compared with those induced by plane waves, it is not clear as to how the wave loads induced by short-crested waves on vertical cylinders with arbitrary cross-sections compare to the wave loads induced by plane waves on the same cylinders. Nor is it clear how the force loading changes with various cylinder cross-sections. Therefore, a study of the effect of short-crested waves incident on vertical cylinders of arbitrary cross-sections seems to be necessary to improve the prediction of wave forces on vertical cylinders.

In this paper, BEM proposed by Au and Brebbia (1983) is adopted to numerically calculate the wave loads due to short-crested waves incident on cylinders of arbitrary cross-sections. Wave loads due to short-crested waves on circular, elliptical and square cylinders will be discussed. Through our study, we found that the wave loads induced by short-crested waves, for a cylinder of certain cross-section, can be larger than those induced by plane waves with the same total wave number.

2. BOUNDARY INTEGRAL FORMULATION

Consider the case that short-crested incident waves travelling in the positive x-direction with the wave potential

$$\Phi^I = \frac{-igA_0}{\omega} \frac{\cosh\{\kappa(z+h)\}}{\cosh(\kappa h)} \exp\{i(\kappa_x x - \omega t)\} \cos(\kappa_y y + \theta), \tag{1}$$

are diffracted by a vertical cylinder resting on the ocean floor and piercing the water surface as shown in Fig. 1. In (1), $i = \sqrt{-1}$, A_0 is the wave amplitude, h is the wave depth, ω is the angular frequency, g is the gravitational acceleration, κ_x, κ_y are wave numbers in the x- and y-directions, respectively, and θ is the phase of the sinusoidal wave crests in the direction perpendicular to the direction of wave propagation. The so-called short-crested waves represented by the wave potential in (1) are travelling in the positive x-direction with celerity

$$C = \left[\frac{g\kappa}{\kappa_x^2} \tanh kd\right]^{1/2}, \tag{2}$$

and the crests are, in the meantime, sinusoidal varying in the y-direction with wave

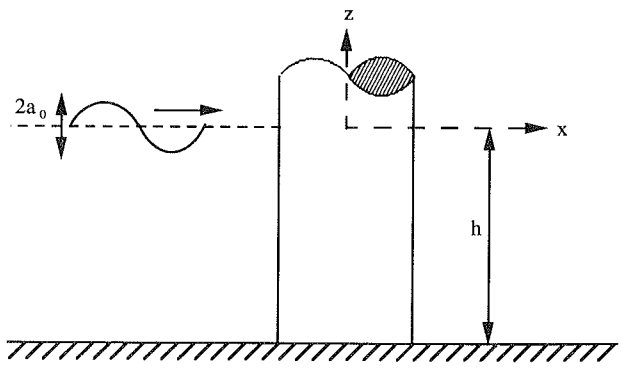

FIG. 1. Waves incident on a vertical cylinder.

number κ_y. κ in the dispersion relation (2) is directly related to the wave numbers κ_x and κ_y by

$$\kappa = \sqrt{\kappa_x^2 + \kappa_y^2}\,. \tag{3}$$

By varying the wave number in the direction perpendicular to wave propagation, κ_y, the waves can be changed from plane waves (κ_y=0) to very short-crested waves ($\kappa_y \gg \kappa_x$). This wide range of values for the wave numbers can produce waves that behave very differently when diffracted around cylinders, but have the same total wave numbers. The phase of the wave perpendicular to the direction of propagation, θ, can also be varied, so that, for example, the crest or the trough can be made to be incident to the middle of a cylinder.

If the direction of wave propagation is of an angle α to the positive x-axis as shown in Fig. 2, a general wave potential for the short-crested incident waves can be written as

$$\Phi^I = \frac{-iga_0}{\omega}\frac{\cosh\{\kappa(z+h)\}}{\cosh(\kappa h)}\exp\{i(\kappa_x^x x + \kappa_x^y y - \omega t)\}\cos(-\kappa_y^x x + \kappa_y^y x + \theta), \tag{4}$$

where

$$\kappa_x^x = \kappa_n \cos(\alpha), \quad \kappa_x^y = \kappa_n \sin(\alpha),$$
$$\kappa_y^x = \kappa_t \sin(\alpha), \quad \kappa_y^y = \kappa_t \cos(\alpha),$$

with κ_n and κ_t being the wave numbers in the direction of wave propagation and the direction perpendicular to the direction of wave propagation, respectively.

The governing equations and the boundary conditions of the scattered wave field, with the assumption that sea water is inviscid and incompressible and flow is irrotational, are

$$\nabla^2\phi + \kappa^2\phi = 0\,, \tag{5}$$

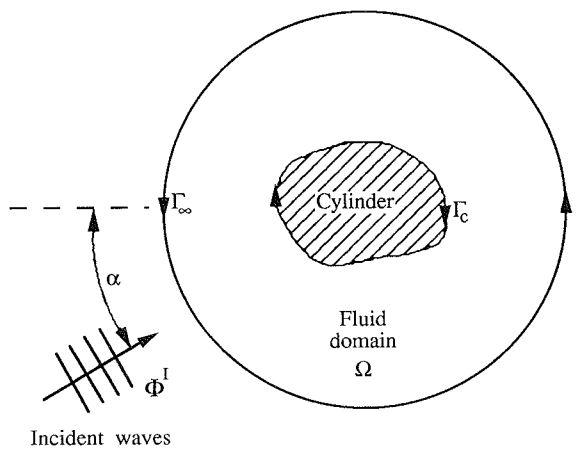

FIG. 2. Boundaries around the fluid domain.

subject to the following boundary conditions

$$\frac{\partial \phi}{\partial n} = -\frac{\partial \phi^{(I)}}{\partial n}, \qquad \text{on } \Gamma_c, \tag{6}$$

$$\frac{\partial \phi}{\partial n} - i\kappa\phi = 0, \qquad \text{on } \Gamma_\infty, \tag{7}$$

in which Γ_c indicates the boundary formed by the surface of the cylinder, Γ_∞ stands for an imaginary boundary at infinity, as shown in Fig. 2, and n is the coordinate in the direction of the unit outward vector $\mathbf{n}$ normal to Γ_c and Γ_∞. Boundary condition (6) states that waves are totally reflected on the surface of the cylinder. Boundary condition (7) is the Sommerfeld radiation condition (see Sommerfeld, 1949), which simply states that the energy associated with the scattered waves will propagate towards infinity without being reflected back. Notice that the scattered waves are of the same angular frequency ω.

Following Au and Brebbia (1983), an approximate solution is sought after the Galerkin weighted residual statement for the governing Equation (5) subject to the boundary conditions (6) and (7) is constructed as

$$\int_\Omega (\nabla^2\phi + \kappa^2\phi)\phi^* \mathrm{d}\Omega = \int_{\Gamma_c} \left(\frac{\partial \phi}{\partial n} + \frac{\partial \phi^{(I)}}{\partial n}\right)\phi^* \, \mathrm{d}\Gamma + \int_{\Gamma_\infty} \left(\frac{\partial \phi}{\partial n} - i\kappa\phi\right)\phi^* \, \mathrm{d}\Gamma, \tag{8}$$

where ϕ^* is a properly chosen weighting function.

As shown by Au and Brebbia, the choice of the weighting function in terms of the Hankel function of the first kind and of zero order, H_0^1, simplifies the final integral equation because the Sommerfeld radiation condition is satisfied at infinity and the integral on Γ_∞ disappears after integration by parts twice on (8). The final integral equation is of the form

$$c_i\phi_i + \int_{\Gamma_c} \left(\phi \frac{\partial \phi^*}{\partial n} + \phi^* \frac{\partial \phi^{(I)}}{\partial n}\right) \mathrm{d}\Gamma = 0, \tag{9}$$

in which

$$c_i = 1 - \frac{\alpha}{2\pi}, \tag{10}$$

with α being the angle between the edges of the two adjacent boundary elements at the point "i" under consideration and ϕ^* is chosen as

$$\phi^* = \frac{i}{4} H_0^1(\kappa r). \tag{11}$$

After the boundary Γ_c is discretized into N boundary elements, the unknown function ϕ can be found by solving (9) and all the other physical properties such as water run-up, the total wave-induced force and moment can be readily calculated.

3. COMPUTATIONAL RESULTS AND DISCUSSION

3.1. *Short-crested waves incident on a circular cylinder*

In order to verify the numerical results and check the convergence of the numerical scheme, the numerical solution for short-crested waves incident on a circular cylinder was carried out first. For this case, an analytic solution was found by Zhu (1993). Therefore, a few particular cases were studied and the wave-induced forces on a circular cylinder were computed numerically and compared with those obtained from the analytical solution. Constant elements were used for good numerical efficiency and satisfactory numerical accuracy (see Au and Brebbia, 1983). In all the numerical calculations we have carried out so far, the water depth and the radius of the cylinder were chosen to be 50 and 10 m, respectively. However, since only the nondimensional force is plotted, the water depth is irrelevant in all the figures shown in this paper.

In Fig. 3, with κ_x being kept constant while κ_y was varied, the nondimensional wave forces from both the analytical solution (solid line) and numerical solution with different number of elements are shown. The convergence of the numerical scheme can be clearly seen as the number of elements is increased. Satisfactory numerical results were obtained when 24 elements were used.

Figure 4 shows the result of varying the two wave numbers, κ_x and κ_y, while keeping the total wave number constant. It is apparent that the total wave force on the cylinder varies linearly with the wave number perpendicular to the direction of propagation (all three lines are straight lines passing through the origin). These numerical results are identical to the analytic results obtained by Zhu (1993).

Unlike plane waves, forces induced by short-crested waves may vary with the phase angle θ in (4). Figures 5–7 show the results for different combinations of wave numbers κ_x and κ_y, with κa being kept to be equal to unity when the wave phase θ is varied.

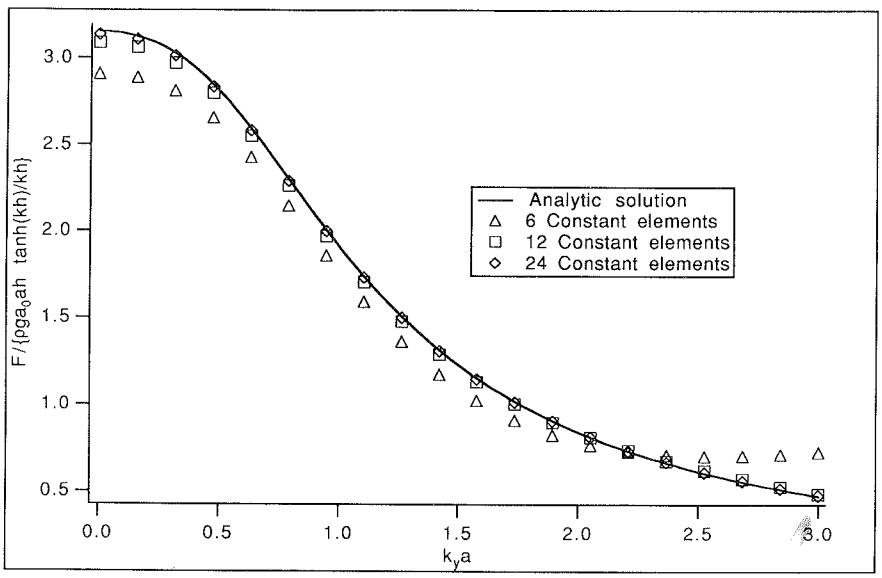

FIG. 3. Short-crested waves incident on a circular cylinder ($\kappa_x a = 0.5$).

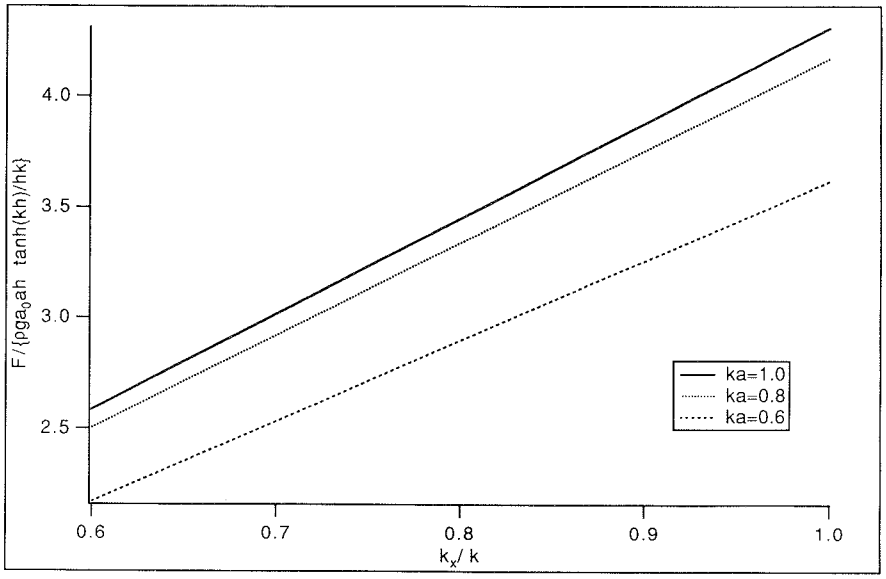

FIG. 4. Short-crested waves incident on a circular cylinder.

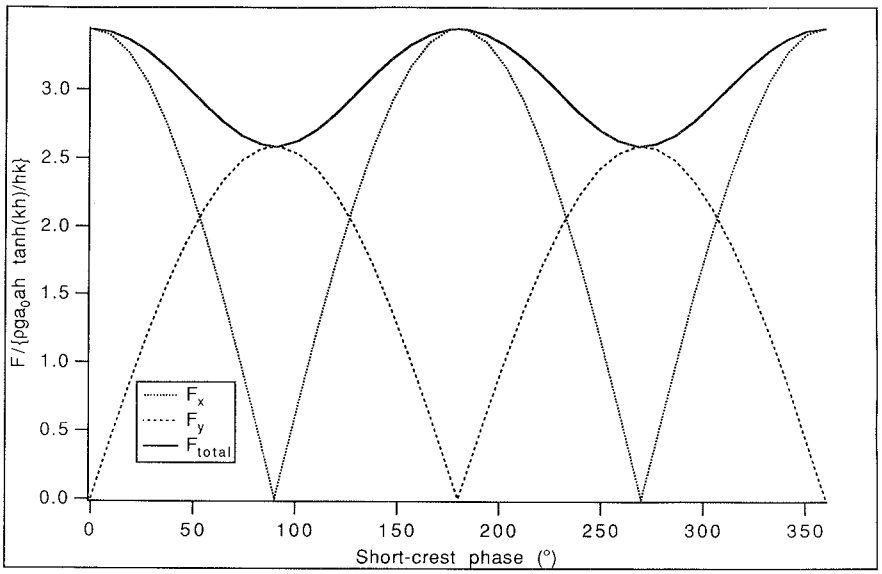

FIG. 5. Short-crested waves incident on a circular cylinder ($\kappa_x a = 0.8$, $\kappa_y a = 0.6$).

From Figs 5 and 7, it can be seen that the total wave force on the cylinder varies sinusoidally with the wave phase, whereas the two force components exhibit cusps at their minima. In the case that $\kappa_x < \kappa_y$, the maximum total wave force is larger than that presented by Zhu (1993), who only discussed the wave-induced forces for $\theta = 0$.

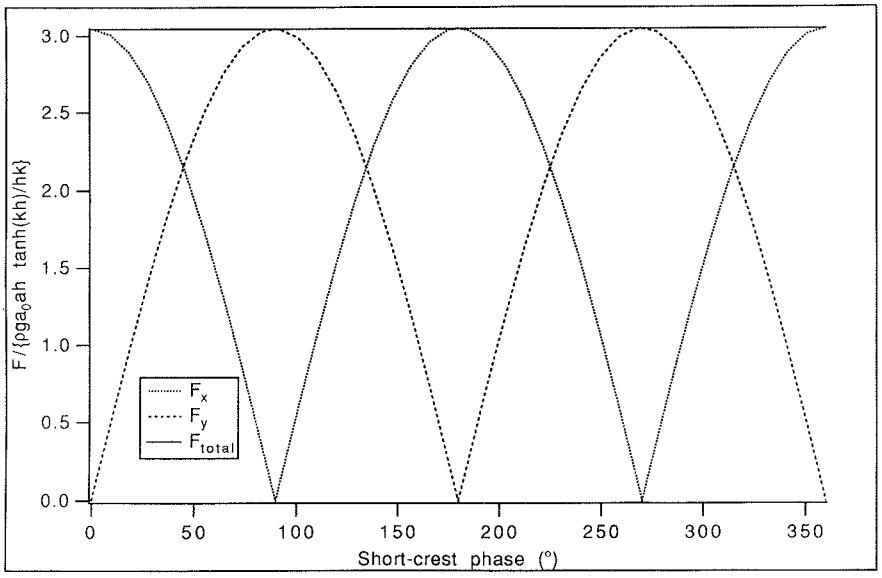

FIG. 6. Short-crested waves incident on a circular cylinder ($\kappa_x a = \kappa_y a = 0.7071$).

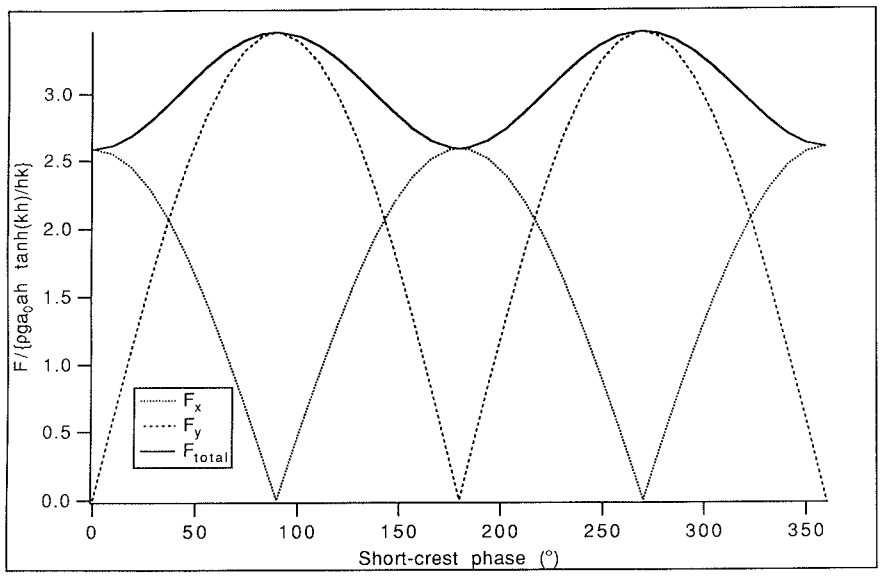

FIG. 7. Short-crested waves incident on a circular cylinder ($\kappa_x a = 0.6$, $\kappa_y a = 0.8$).

However, for circular cylinders, the largest wave-induced forces are still smaller than those induced by plane waves with the same total wave number.

Furthermore, it can be seen from Figs 5 to 7 that the x- and y-components of the wave-induced force all exhibit the same pattern of variation as θ varies from 0 to 360°, whereas the total wave forces have their minima and maxima at different angles θ

depending on $\kappa_x > \kappa_y$, $\kappa_x = \kappa_y$, or $\kappa_x < \kappa_y$. For the force component in the direction of wave propagation, maxima are always reached when θ is 0 or 180°. The y-direction force exhibits the opposite behaviour, having maximum values at a phase of 90 or 270°. The values of 90 and 270° are significant because at these values, the mid-points between the crests and troughs of the incident waves are in line with the centre of the cylinder and there exists a larger difference in wave heights, through the centre of the cylinder, in the direction normal to the direction of wave propagation. Naturally, the y-component of the wave-induced force, which results from the pressure difference on both sides of a cylinder, is expected to be at its maximum in these cases. At zero phase the wave heights are symmetric about the cylinder in the direction of wave propagation and therefore there exists zero net force in the y-direction. For total wave forces, maxima are reached at θ =90 and 270° when $\kappa_x < \kappa_y$, whereas minima are reached at the same phase angles when $\kappa_x > \kappa_y$. For $\kappa_x = \kappa_y$, the total wave force becomes a constant, which simply results from the full symmetry of both the cylinder and the incident wave field in all directions. It is interesting to note that if the total forces for the cases where $\kappa_x < \kappa_y$ and $\kappa_x > \kappa_y$ are averaged across the range of short-crested wave phases, they are equal to the total wave force when $\kappa_x = \kappa_y$.

3.2. *Short-crested waves incident on an elliptical cylinder*

Unlike a circular cylinder, an elliptical cylinder is no longer symmetric in every direction. The diffraction of short-crested waves can therefore be quite different; the conclusion we had for the wave forces experienced by a circular cylinder may not be true any more. A study of the diffraction around an elliptical cylinder is certainly of great interest.

Now, consider the case that with the same incident short-crested waves described by (4), an elliptical cylinder with its major axis being twice that of its monor axis, which is 5 m, has replaced the circular cylinder in Fig. 1. The wave forces in the x- and y-directions were calculated again with constant boundary elements.

With an elliptical cylinder, the variation of the wave-induced force may vary with the angle of incidence, α, in (4). Figures 8 and 9 show the effect of varying the angle of incidence of short-crested waves on an elliptical cylinder. Two different sets of wave numbers were used, but the total wave number has been kept the same so that comparisons can be made between the graphs. It can be seen that the variation of the angle of incidence for short-crested waves has a very similar effect regardless of the values of the wave numbers, κ_x and κ_y. These graphs are also very similar in form to that of the same case involving plane waves. Hence it appears that the actual wave type incident on an elliptical cylinder has little effect on the way that the wave forces vary with the incident angle when κ_x and κ_y are changed in such a way that the total wave number is kept the same.

To examine the effect of different wave numbers on an elliptical cylinder, the total wave number was kept constant while κ_x and κ_y were varied. In comparison with Fig. 4, in which the variation of total wave forces on a circular cylinder is plotted, the x- and y-components of wave-induced force as well as the total force on an elliptical cylinder for $\kappa a = 1.0$ are plotted in Fig. 10. The linear relationship between nondimensional force $F/\{\rho g a_0 h \tanh(\kappa h)/\kappa h\}$ and κ_x/κ shown in Fig. 4 no longer exists; a slight nonlinear variation is exhibited with curves bending downward as κ_x/κ increases.

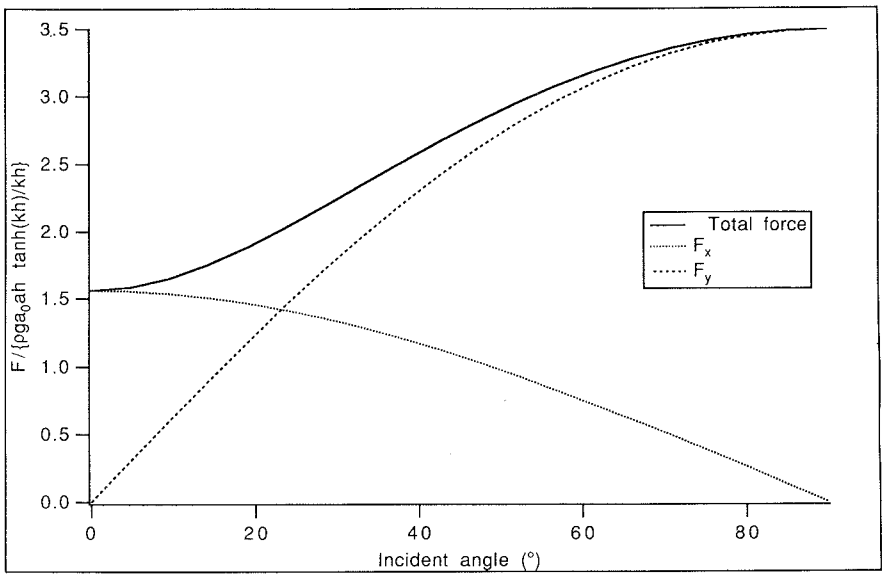

FIG. 8. Short-crested waves incident on an ellipse (axis ratio = 0.5, $\kappa_x a = 0.8$, $\kappa_y a = 0.6$).

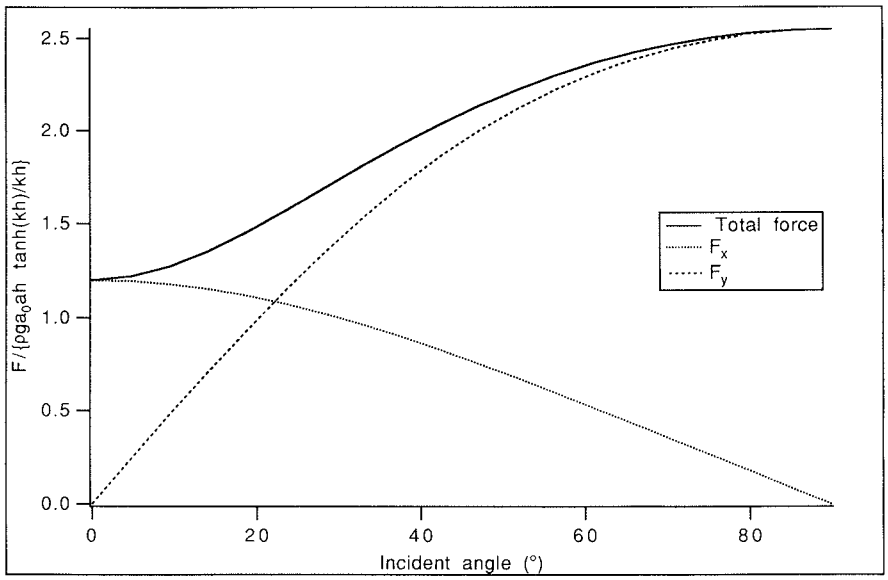

FIG. 9. Short-crested waves incident on an ellipse (axis ratio = 0.5, $\kappa_x a = 0.6$, $\kappa_y a = 0.8$).

However, plane waves with the same total wave number still seem to have induced the largest force on an elliptical cylinder.

Figures 11 and 12 show the effect of varying the phase of the short-crested waves on an elliptical cylinder. These two figures show two different compositions of wave numbers κ_x and κ_y, with the total wave number equalling unity. The graphs show the

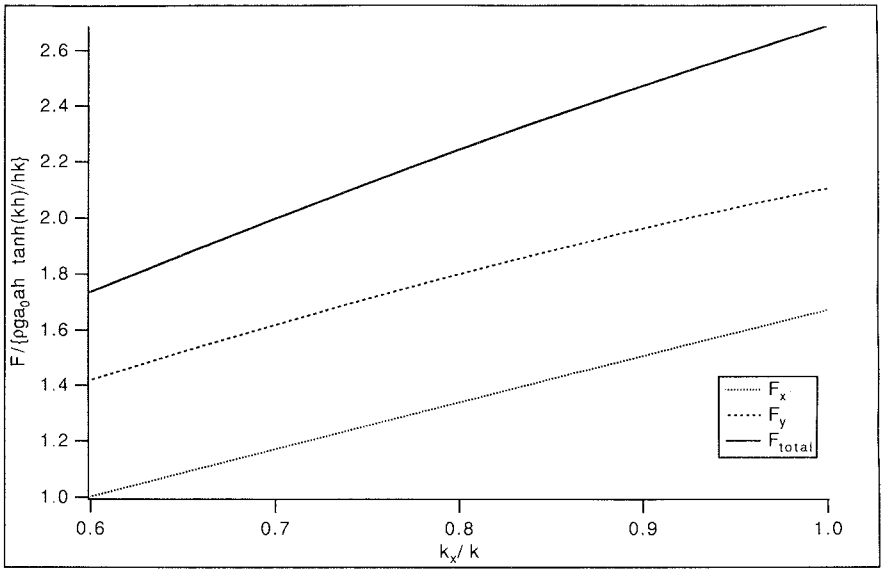

FIG. 10. Short-crested waves incident on an ellipse (κa = 1.0, axis ratio = 0.5, incident angle = 30° to the major axis).

large dependence of the total force on the y-component of the force. This is due to the ellipse having the major axis (which is twice the length of its minor axis) parallel to the x-axis, and hence the surface area facing the y-direction is much larger than that in the x-direction. The difference in wave height on either side of the axis along

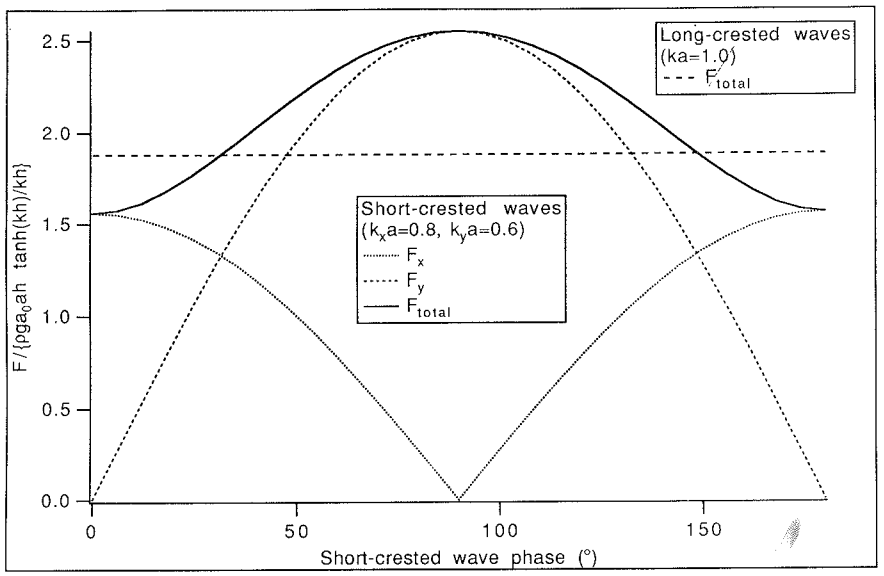

FIG. 11. Waves incident on an ellipse (axis ratio = 0.5, incident angle = 0°).

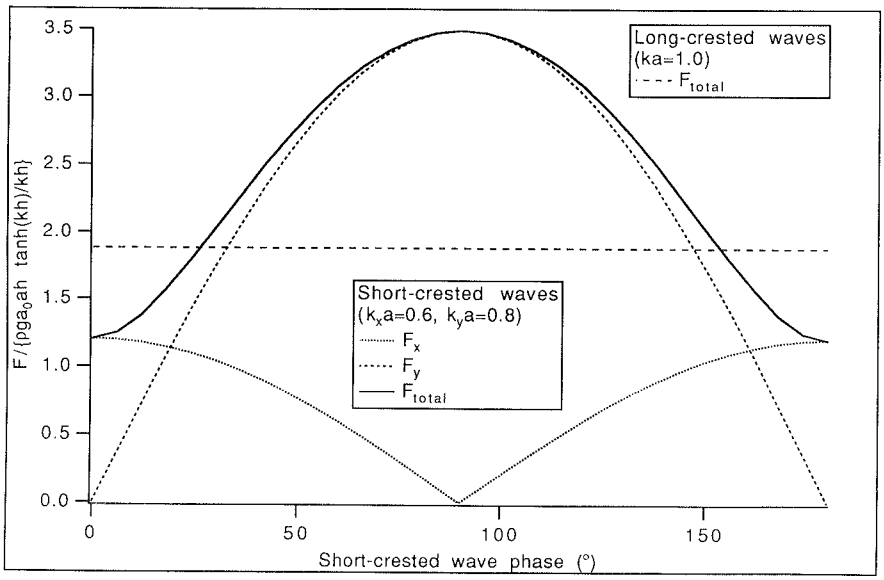

FIG. 12. Waves incident on an ellipse (axis ratio = 0.5, incident angle = 0°).

the direction of wave propagation will have the greatest surface area to act on, and hence will generate the greatest net force. The results of using plane waves with the same total wave number incident on the same cylinder are also plotted on these two figures for comparison (they are indicated by two horizontal dashed lines since there is no lateral phase to vary for plane waves). It is interesting to note that the total wave force due to the short-crested waves exceeds that of the plane waves with the same total wave number for a large range of θ. The maximum total wave force due to short-crested waves increases as the wave number in the direction perpendicular to the direction of wave propagation increases. These results suggest that the forces due to short-crested waves must be taken into consideration when designing non-circular cylinders to withstand ocean waves. This is of great significance, especially to ocean engineers, since most wind-generated waves in the ocean are short-crested rather than plane waves.

In order to illustrate the effect of the incident angle on the forces on the cylinder when the phase of the short-crested waves is also varied, the nondimensional force vs phase angle θ, with the incident angles being set to 30 and 60°, respectively, are plotted in Figs 13 and 14. From these two figures, together with Fig. 11, which is similar to Figs 13 and 14 except that the incident angle is zero, it can be seen that the variations of the total forces due to short-crested waves are quite different for different incident angles. For zero incident angle, the maximum total wave force is reached when the phase angle is 90°, whereas the minimum total wave force is reached at the same phase angle when the incident angle is 60°. When the incident angle becomes 30°, very slight changes are observed when the phase angle is varying from 0 to 180°. All these changes of the total wave force vs the wave phase angle with different incident angles show the complexity of the diffraction of short-crested waves around an object without symmetry in all directions.

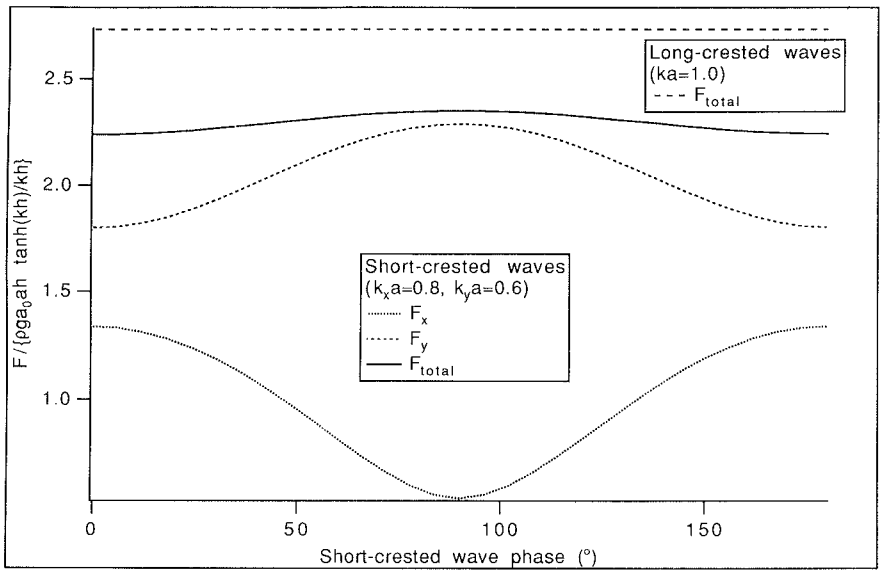

FIG. 13. Waves incident on an elliptical cylinder (axis ratio = 0.5, incidence angle = 30°).

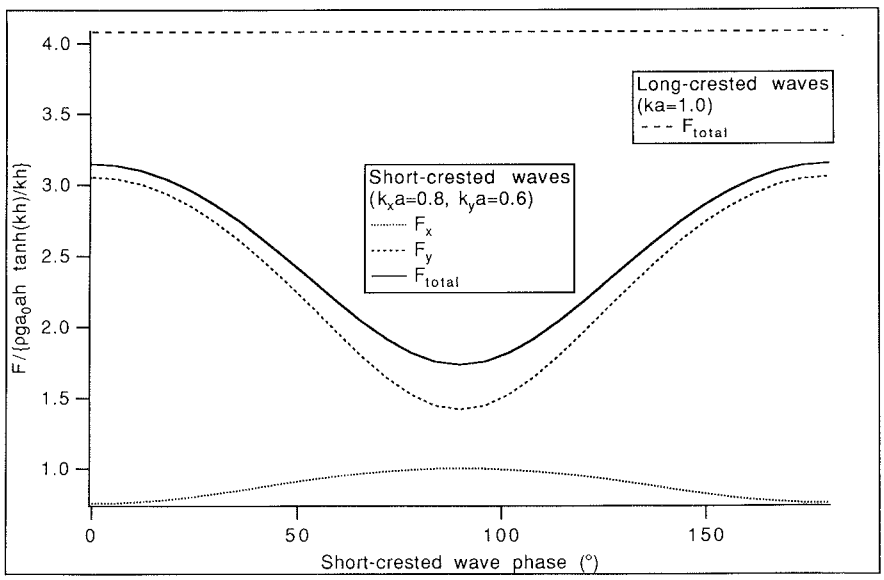

FIG. 14. Waves incident on an elliptical cylinder (axis ratio = 0.5, incidence angle = 60°).

3.3. *Short-crested waves incident on a square cylinder*

It is very interesting to compare the wave-induced forces due to short-crested waves and plane waves on a square cylinder. For plane incident waves, Au and Brebbia (1983) compared their numerical results with the experimental results obtained by

Mordridge and Jamieson (1976) and found that the magnitude of the wave-induced force on a square cylinder is only slightly altered when the angle of incidence changes. Whether or not the same conclusion can be drawn needs to be examined with regard to short-crested waves.

As illustrated in Fig. 15, the forces due to short-crested waves on a square cylinder vary as the angle of incidence is changed. The nondimensional total force changes by about 25% when the incident angle is changed from 0 to 45°, whereas less than 3% of such variation was found for plane incident waves (see Au and Brebbia, 1983). From Fig. 15, it can also be seen that the total force is at the maximum when the angle of incidence is zero, and decreases to the minimum when the waves are directly incident on a corner of the cylinder. This is in contrast to the variation in force due to plane waves incident on a square cylinder where the minimum force occurs when the angle of incidence is zero (see Fig. 16).

The slight nonlinear variation between nondimensional force $F/\{\rho g a_0 h \tanh(\kappa h)/\kappa h\}$ and κ_x/κ when the total wave number κ is fixed exists as well for a square cylinder. Figure 17 shows the horizontal forces on a square cylinder due to short-crested waves incident at 30° while varying the wave numbers such that the total wave number remains constant. In contrast to the variation of the total force on an elliptical cylinder (see Fig. 10), the variation of the total force vs the ratio κ_x/κ is again slightly nonlinear but bending upward as κ_x/κ increases. Again, one cannot jump to the conclusion that plane waves will always induce the largest force on a square cylinder without examining the force variation with the phase of the incident short-crested waves.

With the angle of incidence being 0 and 30°, respectively, Figs 18 and 19 show that the variation of the total force on a square cylinder vs the phase change is sinusoidal in form, with the maximum total forces occurring when the phase angles of the short-

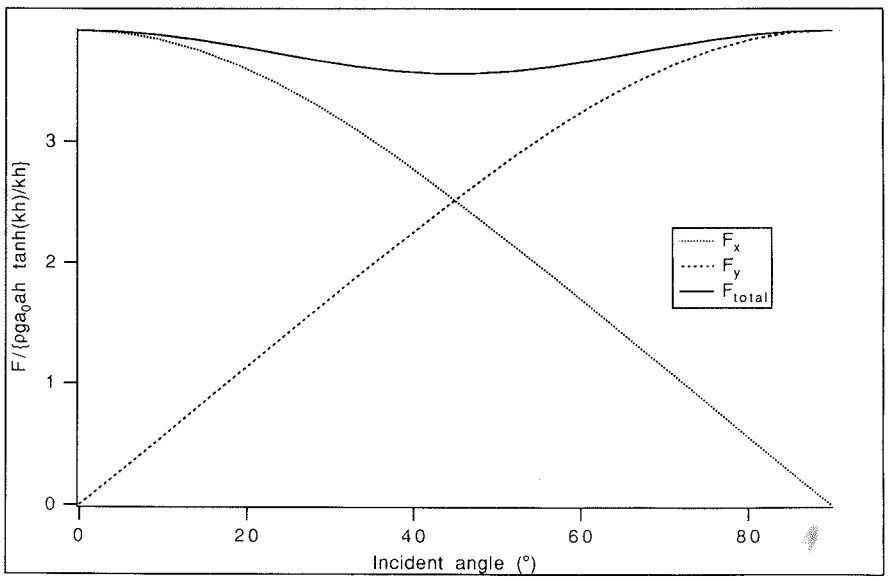

FIG. 15. Force due to short-crested waves incident on a square cylinder ($\kappa_x a = \kappa_y a = 0.7071$).

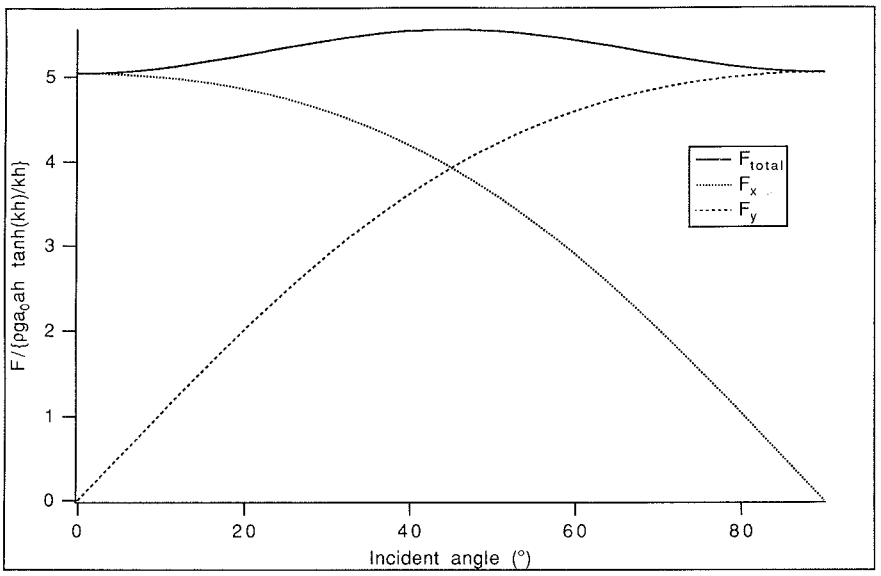

FIG. 16. Force due to plane waves incident on a square cylinder ($\kappa a = 1$).

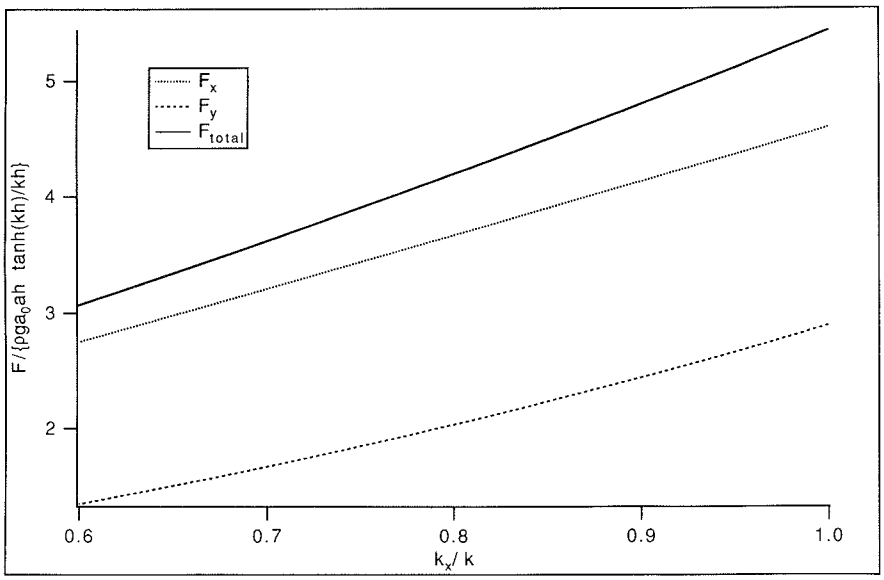

FIG. 17. Force due to short-crested waves incident on a square cylinder at 30° ($\kappa a = 1$).

crested waves are at 90 and 270°. This is similar to the behaviour of the variation in the forces on a circular and an elliptical cylinder when the wavelength in the direction of wave propagation is longer than that in the direction perpendicular to wave propagation (see Figs 7 and 12). It is very interesting to note that there are again cusps, in Fig. 18, on the curves for the two force components when they reach their minima,

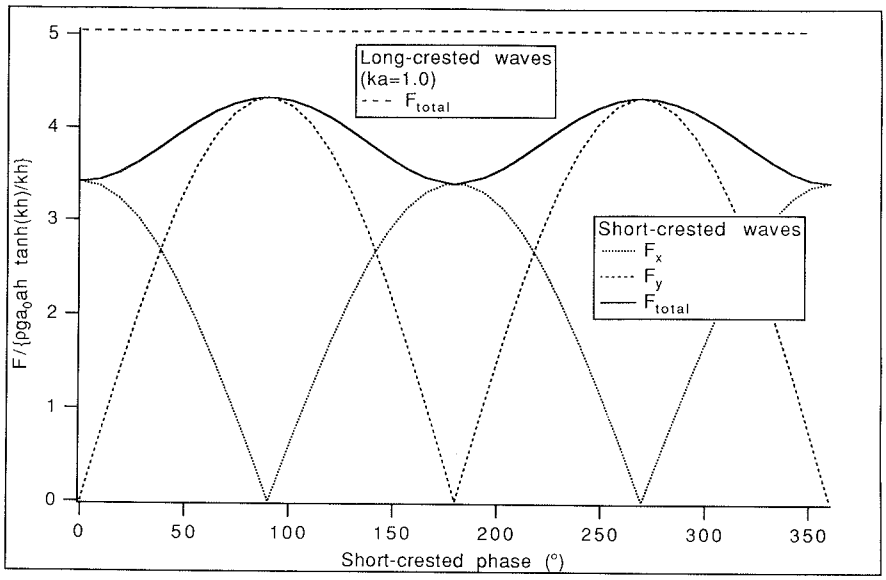

FIG. 18. Short-crested waves incident on a square cylinder ($\kappa_x a = 0.6$, $\kappa_y a = 0.8$, angle of incidence =0°).

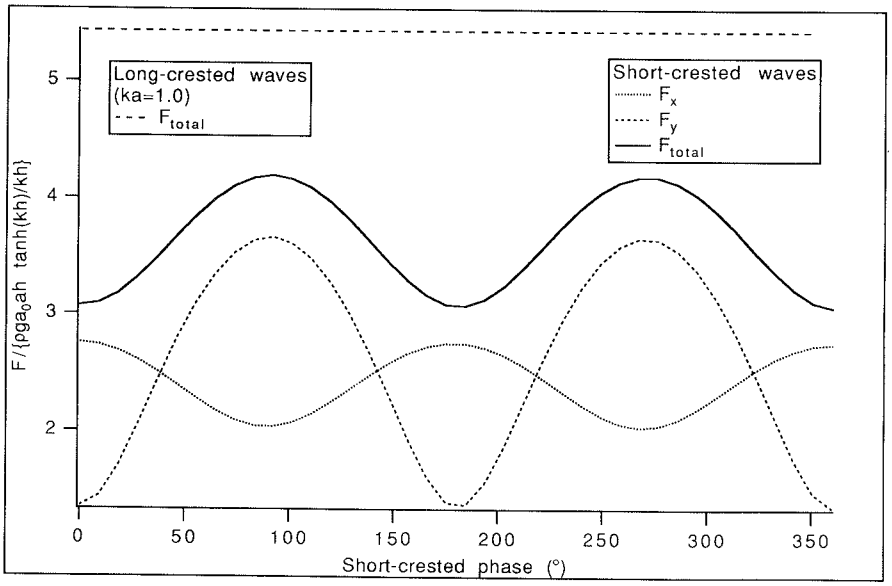

FIG. 19. Short-crested waves incident on a square cylinder ($\kappa_x a = 0.6$, $\kappa_y a = 0.8$, angle of incidence = 30°).

whereas there are no such cusps when they reach their maxima. However, there are no sudden changes in the total wave-induced force because when one component reaches its minimum, the other one is always at its maximum. Similar cusps on the curves for the two force components have already been observed in Figs 5–7 for the forces on a circular cylinder and in Figs 11 and 12 for the forces on an elliptical cylinder

with zero incident angles. On the other hand, these cusps on the curves for the two force components seem to have disappeared when the angle of incidence becomes 30° (see Fig. 19). Interestingly, there are also no cusps on the curves for the two force components in Figs 13 and 14 for an elliptical cylinder with the incident angle being non-zero. For a square cylinder, the total force due to plane waves (incidated by a horizontal dashed line) appears to be always greater than the forces due to short-crested waves with the same total wave number.

4. CONCLUSIONS

In this paper, the wave-induced forces due to short-crested incident waves on vertical cylinders with different cross-sections are discussed. The numerical results for the wave-induced forces on the cylinders due to the diffraction of short-crested waves were obtained by solving an integral equation with the boundary element method. Good agreement between the numerical solution and analytical solution for the case of a circular cylinder has been demonstrated with only 24 constant elements being adopted.

For cylinders with non-circular cross-sections, the total wave forces depend not only on the angle of incidence, but also on the phase of the incident short-crested waves in the direction perpendicular to wave propagation. Quite different variations of the total forces on an elliptic cylinder and on a square cylinder have been observed in our numerical experiments when the phase in the direction perpendicular to the direction of wave propagation is varied.

It is found that short-crested and plane waves behave very differently with regard to the wave loading on a cylinder. The results indicate that in some cases the forces due to short-crested waves can exceed those of plane waves with the same total wave number. The wave-induced forces due to short-crested waves can be larger for non-circular cylinders. Hence, for the design of off-shore structures the effect of short-crested incident waves also needs to be examined, due to their complex behaviour when being diffracted around vertical cylinders of arbitrary cross-sections.

REFERENCES

AU, M.C. and BREBBIA, C.A. 1983. Diffraction of water waves for vertical cylinders using boundary elements. *Appl. Math. Modelling* **7,** 106–114.

BANAUGH, R.P. and GOLDSMITH, W. 1963. Diffraction of steady acoustic waves by surfaces of arbitrary shapes. *J. acoust. Soc. Am.* **35,** 1590–1601.

BETTESS, P. and ZIENKIEWICZ, O.C. 1976. Diffraction and refraction of surface waves using finite and infinite elements. *Int. J. Num. Meth. Engng* **11,** 1271–1290.

BREBBIA, C.A., TELLES, J.C.F. and WROBEL, L.C. 1984. *Boundary Element Techniques: Theory and Applications in Engineering.* Springer, Berlin.

CHAKARBARTI, S.K. and TAM, A. 1975. Interaction of waves with large vertical cylinder. *J. Ship Res.* **19,** 22–23.

CHEN, H.S. and MEI, C.C. 1974. Oscillations and wave forces in a man-made harbor in the open sea. In *Proceedings of the 10th Symposium on Naval Hydrodynamics, Cambridge, Massachusetts,* pp. 573–596.

FUCHS, R.A. 1952. On the theory of the short-crested oscillatory waves: gravity waves. National Bureau of Standards Circular No. 8, pp. 187–200.

GODA, Y. AND YOSHIMURA, T. 1972. Wave force on a vessel tied at off-shore dolphins. In *Proceedings of the 13th Coastal Engineering Conference,* Vol. III, ch. 96, pp. 1723–1742.

HOUSTON, J.R. 1981. Combined refraction and diffraction of short waves using the finite element method. *Appl. Ocean Res.* **3,** 163–170.

HSU, J.R.C., TSUCHIYA, Y. and SILVESTER, R. 1979. Third-order approximation to short-crested waves. *J. Fluid Mech.* **90,** 179–196.

HWANG, L.S. and TUCK, E.O. 1970. On the oscillations of harbours of arbitrary shape. *J. Fluid Mech.* **42,** 375–394.

JEFFREYS, H. 1924. On water waves near the coast. *Phil. Mag., ser. 6* **17,** 44–48.

LEE, J.J. 1971. Wave induced oscillation in harbours of arbitrary geometry. *J. Fluid Mech.* **45,** 375–394.

MACCAMY, R.C. and FUCHS, R.A. 1954. Wave forces on piles: a diffraction theory. U.S. Army Corps of Engineering, Beach Erosion Board, Technical Memorandum No. 69.

MEI, C.C. 1978. Numerical methods in water-wave diffraction and radiation. *Ann. Rev. Fluid Mech.* **10,** 393–416.

MODRIDGE, G.R. and JAMIESON, W.W. 1976. Wave forces on square caissons. In *Proceedings of the 135th Coastal Engineering Conference AMSE,* ch. 133, pp. 2271–2289.

NEELAMANI, S., SUNDAR, V. and VENDHAN, C.P. 1989. Dynamic pressure distribution on a cylinder due to wave diffraction. *Ocean Engng* **16,** 343–353.

SOMMERFELD, D. 1949. *Partial Differential Equations in Physics.* Academic Press, New York.

TSAY, T.-K. and LIU, P.L.-F. 1983. A finite element model for wave refraction and diffraction. *Appl. Ocean Res.* **5,** 30–37.

TSAY, T.-K., ZHU, W. and LIU, P.L.-F. 1989. A finite element model for wave refraction, diffraction, reflection and dissipation. *Appl. Ocean Res.* **11,** 33–38.

YUE, D.K.P., CHEN, H.S. and MEI, C.C. 1976. Water wave forces on three-dimensional bodies by a hybrid element method. Technical Report, 215 MIT, Department of Civic Engineering, Parsons Laboratory (p. 222).

ZHU, S.-P. 1993. Diffraction of short-crested waves around a circular cylinder. *Ocean Engng* **20**, 389–407.